BOLLETTINO DELLA SOCIETÀ GEOGRAFICA ITALIANA

Firenze University Press
www.fupress.com/bsgi

OPEN ACCESS

Citation: A. Favretto (2018) Urban Heat Island analysis with Remote Sensing and GIS methods: an application in the Trieste area (North-East of Italy). *Bollettino della Società Geografica Italiana* serie 14, 1(1): 215-229. doi: 10.13128/bsgi.v1i1.101

Data Availability Statement: All relevant data are within the paper and its Supporting Information files.

Competing Interests: The Author(s) declare(s) no conflict of interest.

Urban Heat Island analysis with Remote Sensing and GIS methods: an application in the Trieste area (North-East of Italy)

Analisi di isole di calore urbane con il telerilevamento in ambiente GIS: un'applicazione nella Provincia di Trieste

Andrea Favretto

Dipartimento di Studi umanistici, Università di Trieste, Italia
E-mail: afavretto@units.it

Abstract. It is well-known that many factors increase urban outdoor temperature. Urban landscapes and buildings designs that do not consider this specific issue are probably the most important causes of the so-called Urban Heat Island effect (UHI). Furthermore, loss of vegetation and of pervious surface cover can increase the intensity of the UHI effect. Specialist knowledge of the UHI growth factors and their impact on the urban microclimate is of the upmost importance for the adoption of efficient mitigation measures. This paper uses Remote Sensing and GIS methods in order to investigate the main UHI impact factors in the Province of Trieste (the capital of the Friuli Venezia Giulia Region, North-East of Italy). With this aim, the surface temperature is considered from a medium spatial resolution remote sensed image and these data are cross-checked with the local albedo, the urban vegetation and the building density. The main results of the paper are of a geographical kind. The remote sensing methods showed that, in the area studied, there was a strong correlation between higher temperatures and building density and the absence of vegetation. This is particularly evident in the urban environment of the city of Trieste (but it also occurs in the small villages of the surrounding area).

Keywords: Urban Heat Island (UHI), surface temperature, vegetation index, building density.

Riassunto. È noto che sono diversi i fattori che possono incrementare le temperature in ambito urbano. Le strutture urbane che non tengono conto del loro possibile impatto sulla temperatura esterna sono probabilmente la maggiore fonte delle cosiddette "isole di calore urbane". La diminuzione della vegetazione cittadina, unita a quella delle superfici permeabili di copertura del suolo possono aumentare ulteriormente la temperatura delle città. La conoscenza dei fattori che determinano le isole di calore urbane e dei loro effetti sul microclima cittadino è di grande importanza al fine dell'adozione di efficienti politiche di mitigazione del fenomeno. Il contributo impiega tecniche del Telerilevamento in ambiente GIS per lo studio dei principali fattori che incrementano la temperatura urbana nella Provincia di Trieste (capoluogo della Regione Friuli-Venezia Giulia). A tal riguardo la temperatura di superficie, ottenuta da un'immagine a media risoluzione spaziale del satellite Landsat 8, è incrociata con le capacità riflettenti

del suolo e del costruito urbano, con la vegetazione cittadina e la densità del costruito. I principali risultati del lavoro sono di carattere geografico. Si è trovata una forte correlazione fra alte temperature urbane, densità del costruito e assenza di vegetazione. Tale fenomeno è di particolare intensità nel centro urbano di Trieste ma si nota anche nei paesi dell'entroterra carsico.

Parole chiave: isole di calore urbano, temperature urbane, indice di vegetazione, densità del costruito.

1. Introduction

The Urban Heat Island (UHI) effect is a commonly used term to indicate "the tendency of urban areas to experience higher outdoor temperature levels (up to 12 K higher) compared to their contiguous rural periphery" (Aleksandrowicz et al. 2017). Nowadays, more than half of the world's population lives in urban settlements and by 2030 "urban areas are projected to house 60 percent of people globally and one in every three people will live in cities with at least half a million inhabitants" (UN 2016). Therefore, UHI may well be considered a global issue, which "threatens the operation and habitability of our cities and urban environments" (Mohajerani et al. 2017) and will have implications for human comfort and health, urban air pollution, energy management and urban planning (de Faria Peres et al. 2018).

The causes of UHI are connected to the urbanization processes and the improper planning of cities (Nuruzzaman 2015). These processes lead to the creation of densely situated buildings and surfaces like concrete and asphalt, with heat retaining properties (Harlan et al. 2011; Mavrogianni et al. 2011). The result is high heat emissions (Santamouris 2011) and creates a greater demand for energy to cool buildings (Adinna et al. 2009). Furthermore, the high density of urban street canyons (Smith et al. 2008), the lack of green areas and the profusion of areas with reduced permeability and low albedo materials can play an active role in UHI (Taha 1997), together with reduced wind speed caused by the geometry of the city buildings (O'Malley et al. 2014).

UHI intensity may differ seasonally because of differences in local climate and the vegetation cover (Yang et al. 2013; Sun et al. 2007). The phenomenon is best observed under relatively undisturbed meteorological conditions (Gondocs et al. 2017).

The battle against UHI involves a variety of actions, commonly known as adaptation and mitigation measures, terms also used in climate change terminology (Aleksandrowicz et al. 2017). The first ones are short term adjustments of human behavior and systems (light clothes and/or air conditioning). The mitigation measures aim at the transformation of the urban microclimate through modification of the physical environment. A recent paper that analyzes the current trends in UHI mitigation extrapolated from a large research repository (Aleksandrowicz et al. 2017), identifies several main mitigation measures. These are: "cool building envelopes", "green roofs", "green facades", "shade from trees", "ground vegetation", "water bodies", "cool pavements", "water retentive pavements", "built environment typical section", "built environment orientation to prevailing winds", "built environment orientation to the sun". These mitigation measures can be clustered into four main intervention domains: "building envelope", "urban landscaping", "pavement", and "street geometry".

UHI can be divided into some different categories. Subsurface UHI (SubUHI), indicates the warmth of the urban ground subsurface temperature (SST) against the rural background (Zhan et al. 2014; Menberg et al 2013). Surface urban heat island (SUHI) refers to the warmth of the urban surface (Yuan et al. 2007). Canopy Layer Heat Island (CLHI) refers to the warmth of the urban layer upwards from the surface to approximately mean building height while boundary layer heat island (BLHI) refers to the warmth of the layer located above the canopy layer (Voogt et al. 2003). In this paper we consider SUHI which will be generally named UHI.

Basically, there are two main ways to evaluate the UHI phenomenon: conventional weather station automatic temperature measurements (Tzavali et al., 2015) or the Land Surface Temperature (LST) measurements, given by Thermal InfraRed (TIR) remote sensing data (Weng 2009; Voogt 2003; Mushore et al. 2017; Jiménez-Muñoz et al. 2014; Cristobal et al. 2018).

Many authors have investigated the relation between satellite measured LST and other variables like, for instance: vegetation cover, land surface albedo, the urban spatial structure and its reflective patterns (Roth et al. 1989; Gallo et al. 1993; Bonafoni et al. 2017; Lo et al. 1997; Chen et al. 2006; Grover et al. 2015 and the review article: Voogt et al., 2003). Also wind speed, affected by the urban texture (Yang et al. 2016), and the presence of water bodies have the ability to affect land temperatures (Moyer et al. 2017).

Referring to the vegetation, the relationship between NDVI and temperature has long been recognized. NDVI (Normalized Difference Vegetation Index) is considered one of the major indicators of the urban climate (Gallo et al. 1993; among the most recent: Zhang et al. 2010; Zeng et al. 2010; Keramitsoglou et al. 2011). A negative correlation between NDVI and LST has been indicated (Deng et al. 2018; Yue et al. 2007; Sun et al. 2007). Moreover, this negative correlation was discovered to be

non-linear (Yuan et al. 2007; Amanollahi et al. 2012). The nonlinearity between NDVI and LST suggested that NDVI alone may not be a sufficient metric to study UHI quantitatively (Yuan et al. 2007). Regarding the built-up spatial structure, the urban intensity and the ground imperviousness, they have also been recognized as temperature raising factors (Oke 1976; Weng 2001; Mohapatra et al. 2010). Albedo is a well-known parameter which describes the reflective behavior of a surface (Bonafoni et al. 2017). On the other hand, a less reflective surface is known to be one of the most cited strategies to mitigate UHI (Aleksandrowicz et al. 2017; Nuruzzaman 2015; U.S. Environmental Protection Agency 2008).

Land surface albedo is an important controlling factor for the Earth energy budget because it specifies the amount of solar radiation reflected by the ground (Liang et al., 2010). Satellite measured albedo is also widely used in order to investigate SUHI (Kim 1992; Nichol 2005; Vahmani et al. 2016; Rasul et al. 2017; Weng 2009; Lo et al. 1997; Chen et al. 2006; Bonafoni et al. 2017; Chen et al. 2016; de Faria Peres et al. 2018).

In this paper we tried to investigate how some well-known UHI impact factors ("building density", "albedo", "NDVI") are correlated with the surface temperature in the studied area. Furthermore, we tried to locate, on a thematic map, these UHI impact factors with reference to their effects on the surface temperature. This was realized by an unsupervised classification of the considered UHI impact factors stacked image.

The paper is organized as follows. Firstly, the used satellite scene and the studied area are presented (in the "Materials and Methods" section). Then, the four created thematic layers are presented. They are: "building density", "albedo", "surface temperature – Celsius", "vegetation index – NDVI". These layers are then stacked into one image and classified (in an unsupervised manner). In the following "Results" section, some statistical correlation between the thematic layers is investigated. The "Results" section ends with an attempt to describe the main local UHI features in the studied area (obtained by the unsupervised classification of the four-layer stacked image). The paper finishes with some concluding remarks in the "Discussion" section.

2. Materials and Methods

2.1 The satellite scene used and the studied area

We used a satellite scene acquired by Landsat 8 on 2017-07-06 (WRS/Path/Row: 191/028; CRS-Datum/proj/zone: WGS84/UTM/33).

The image was released by USGS[1] as Climate Data Records (CDR). CDR are "higher-level Landsat data products to support land surface change study" (USGS, 2017), and also include the surface reflectance (SR)[2].

The OLI image used was atmospherically corrected to SR using the Landsat Surface Reflectance Code (LaSRC) algorithm. LaSRC has recently replaced the previous Landsat 8 Surface Reflectance (L8SR, June 2016). The main differences between the LEDAPS and LaSRC algorithms can be read on USGS (2016). One important difference is the data sources for the atmospheric composition, which, in the case of LEDAPS, are from the National Centres for Environmental Prediction (NCEP, http://www.ncep.noaa.gov/) and, in the case of LaSRC, are MODIS remotely sensed data.

The studied area was the Trieste Province (TP). TP is located in the South-Eastern part of the Friuli Venezia Giulia Region (FVG, North East Italy). It is the smallest Italian Province (212 sq. km) and has six municipalities[3]. Trieste, its main town, is the capital of the FVG Region.

TP is predominantly a narrow coastal belt next to the North-Eastern part of the Adriatic Sea (the Gulf of Trieste), which is bordered by the Trieste Karst, a plateau of low rounded hills and low mountains, ranging from 100 or 200 to almost 700 meters above sea level. The vegetation in TP is very rich and complex and is partly Illyrian (of Balkan origin), partly Alpine (and Sub-Alpine) and also contains Mediterranean elements (Poldini et al. 1980).

According to the Köppen-Geiger classification (http://koeppen-geiger.vu-wien.ac.at/), Trieste is characterized by a wet temperate climate with hot summers (https://www.centrometeoitaliano.it/). The mean annual air temperature in recent climatology (1971-2000) was 14.5 degrees Celsius in the city of Trieste while 12.3 degrees in the Karst area. The mean annual precipitation was 986 mm (Trieste) and 1342 mm in the inner Karst plateau. Trieste is often swept by the Bora wind (Burja in Slovenian). This is a katabatic north-easterly to easterly wind blowing from the Karst plateau, which can reach 130 km/h, comes almost every year during the winter time and is associated with very low temperatures.

---

[1] See: ESPA (Earth Resources Observation and Science /EROS Center Science Processing Architecture) on demand interface (https://espa.cr.usgs.gov/).

[2] SR is the satellite derived Top of Atmosphere reflectance (TOA) "corrected for the temporally, spatially and spectrally varying scattering and absorbing effects of atmospheric gases and aerosols" (Vermote et al. 2016).

[3] From 1st January 2017, the provinces of the Friuli Venezia Giulia region have been abrogated (Regional Law n. 26 of the 12 of December 2014). They were definitively dissolved on the 31 October 2017 (see: http://www.provincia.trieste.it/).

Figure 1 shows the Landast 8 image used in a true color composite. The borders of the Trieste Province were overlaid on the raster image.

2.2 Building density layer construction

We used the CTR (Technical Regional Map) of the Friuli Venezia Giulia Region (scale 1:5000). We isolated the "Building" Layer (BL) from all the CTR vector layers. Figure 2 shows a detail of the BL located in the Trieste town center.

Then, we built a point vector layer from the BL by replacing each polygon with its centroid[4] (see Figure 3, where you can see the centroid vector layer overlaid on the BL).

Finally, we produced a density map of the buildings applying the Kernel Density Estimation (KDE) method to the centroid vector layer. KDE produced a raster layer in which each cell represents the centroid density. KDE is a commonly used statistic method in order to estimate a density function on the basis of a statistical sample. The kernel function used is based on Silverman, (Silverman, 1986 – eq. 4.5, page 76). When KDE is applied to a point vector layer, some parameters have to be chosen[5].

Figure 4 shows the density map produced. As you can see from the key, the map range of values is: 0-651.533 (black to white). This means that every raster cell (of 30 meters on a side) has an estimated centroid density of 0-651.533 per square kilometer.

2.3 Albedo layer construction

The estimation of the land surface albedo from remote sensed imagery has continuously improved over the last 30 years and today many satellite products are available for coarse resolution climate modeling appli-

Figure 1. The Landsat 8 image used in a true color visualization. The vector layer showing the border of the Trieste Province is overlaid on the raster scene (yellow).

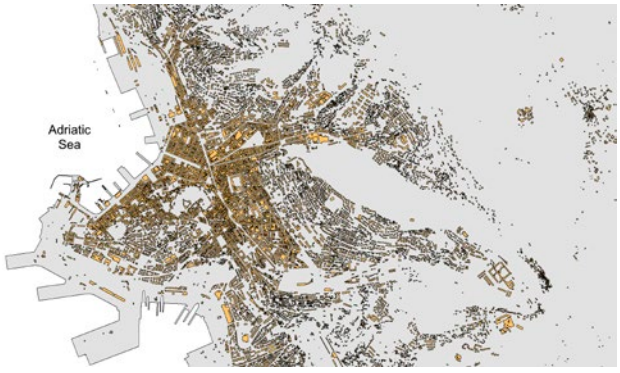

Figure 2. The center of the city of Trieste in the "Building" layer of the Technical Regional Map of the Friuli Venezia Giulia Region (scale 1:5000).

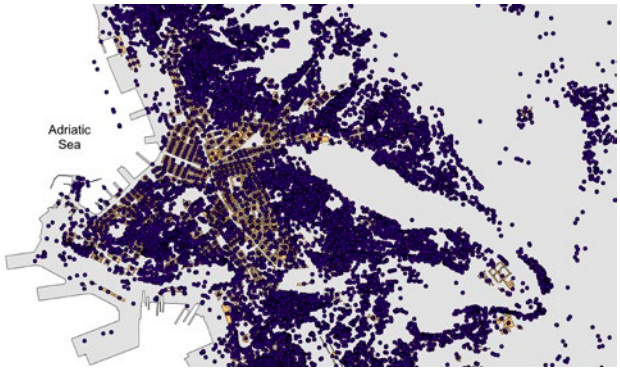

Figure 3. The center of Trieste town. The built centroid vector layer overlaid on the "Building" layer of the Technical Regional Map of the Friuli Venezia Giulia Region (scale 1:5000).

[4] The choice to use the centroids and not the effective size of the buildings may produce generalization problems in the KDE results. In this first stage of our analysis, we decide to use the centroids and not to build a vector map of the effective size of the building. This will be made in a second step, by the elaboration of a more recent ortho-photo of the study area (the used CTR is dated 2003, see: http://www.regione.fvg.it/rafvg/cms/RAFVG/ambiente-territorio/conoscere-ambiente-territorio/FOGLIA4/FOGLIA1/).

[5] The parameters chosen are: the size of the search radius (so called bandwidth), the kernel function, the cell size of the output raster layer. The bandwidth has been computed specifically to the input dataset by the software used (ESRI ArcGIS uses a spatial variant of Silverman's rule of thumb, robust to the spatial outliers – see "How Kernel density works" on ArcGIS 10.5.1 Help). The adopted quartic kernel function allows more smoothed surfaces (Borruso 2008). The cell size, which is generally connected to the case study, was set to 30 meters (the spatial resolution of the Landsat 8 image).

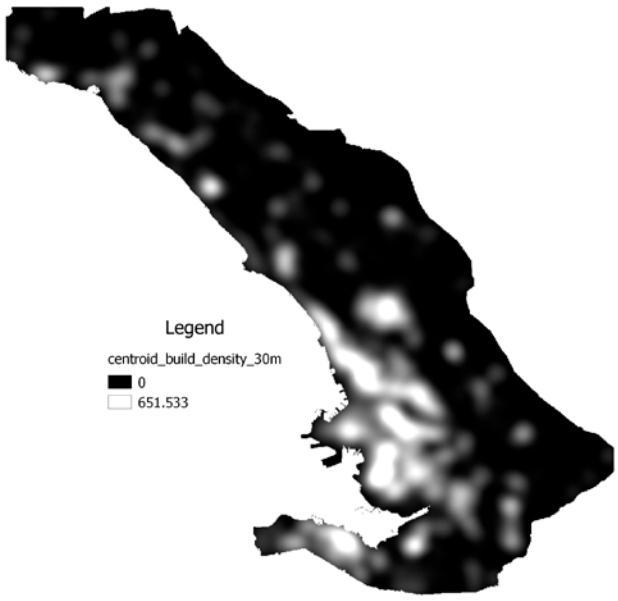

Figure 4. The building density map obtained by the application of the Kernel Density Estimation method to the centroid vector layer (Figure 3).

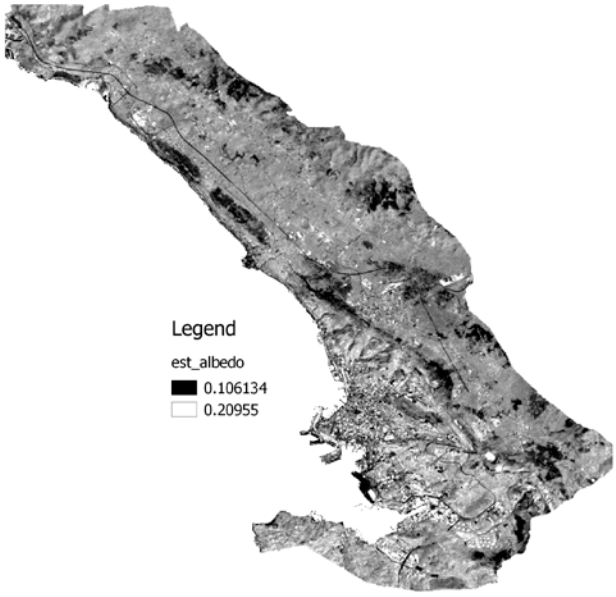

Figure 5. The albedo map of Landsat 8 image (Province of Trieste).

cations (see: He et al., 2018 and its referenced bibliography on coarse resolution climate applications). Albedo estimation from Landsat imagery generally requires starting from surface reflectance instead of Digital Numbers (DN). Surface reflectance is given by atmospheric correction procedures applied to the raw Landsat images (the previous He/2018 quoted paper is a case of an albedo direct estimation approach). Several land surface estimation methods have been developed (Duguay et al. 1992; Brest et al. 1987; Pimentel et al. 2016; da Silva et al. 2016; Baldinelli et al. 2017; Alves et al. 2017).

We used the Yale method for building the albedo layer of the Trieste Province (see: Yale University Center for Earth Observation, https://yceo.yale.edu/how-convert-landsat-dns-albedo). This method comes from the work of Liang (2001). The Liang algorithms for the ETM+ sensor were normalized by Smith (2010) and can also be used for the OLI sensor of Landsat 8 (see: "Yale Guide to Landsat 8 Image Processing" and the all the documentation at: "Yale University/Understanding Landsat 8", https://surfaceheat.sites.yale.edu/understanding-landsat-8).

So we applied the equation (1) to the SR of the OLI bands n.: 2 (blue), 4 (red), 5 (nir), 6 (swir 1) and 7 (swir 2):

(1) [(0.356*band 2)+(0.130*band 4)+(0.373*band 5)+(0.085*band 6)+(0.072*band 7)–0.018]/1.016

Figure 5 shows the estimated albedo map derived from the (1) equation.

2.4 Land Surface Temperature layer construction

USGS delivers (as on demand products) the Top of Atmosphere Brightness Temperature (TOABT). TOABT is derived from Top of Atmosphere radiance and two thermal constants, as described at: https://landsat.usgs.gov/using-usgs-landsat-8-product. TOA radiance is collected by the Thermal Infrared Sensor (TIRS) with two spectral bands (10 and 11) for the wavelength covered by a single band on the previous TM and ETM+ sensors (see: https://landsat.usgs.gov/landsat-8). USGS recommends "that users refrain from relying on band 11 data in quantitative analysis of the TIRS data due to the larger calibration uncertainty associated with this band" (see: https://landsat.usgs.gov/using-usgs-landsat-8-product).

Land Surface Temperature (LST[6]) can be calculated from TOABT. With this aim, we used the equation (2) (Weng et al., 2004):

[6] LST is an important parameter widely used in many disciplines. Among its common applications, UHI monitoring can also be noted. The advent of artificial satellites offered the possibility to get LST over wide areas. However, there is still a trade-off between spatial and temporal resolutions when using satellite data to produce LST because "the resolution cells are larger than the thermal elements" (Zhan et al. 2013; Chen et al. 2017).

(2) $T = TB / [1 + (\lambda * TB/c2) * \ln(e)]$

where:
T = LST
TB = TOABT
λ = wavelength of emitted radiance (for Landsat 8 TIRS band 10 is the center wavelength of the interval: 10.60 – 11.19 micrometers)
$c2 = h * c/s = 1.4388 * 10^{-2}$ m K
h = Planck's constant = $6.626 * 10^{-34}$ J s
s = Boltzmann constant = $1.38 * 10^{-23}$ J/K
c = velocity of light = 2.998 * 108 m/s
e = Land Surface Emissivity (LSE) of each Landsat image pixel

LSE is a surface parameter derived from the emitted radiance measured from space. There are several proposed methods to achieve this aim (for a complete review of LSE retrieval methods, see: Li et al., 2013).

In order to calculate LSE, we classified the Landsat 8 image in four landcover classes: "Grass", "Soil", "Asphalt/Concrete", "Water". Then we reclassified each landcover value with its emissivity value, extracted from Wittich (1997): "Grass" - 0.982; "Soil" - 0.928; "Asphalt/Concrete" - 0,9395; "Water" – 0,92.

Figure 6 shows LST calculated as described above.

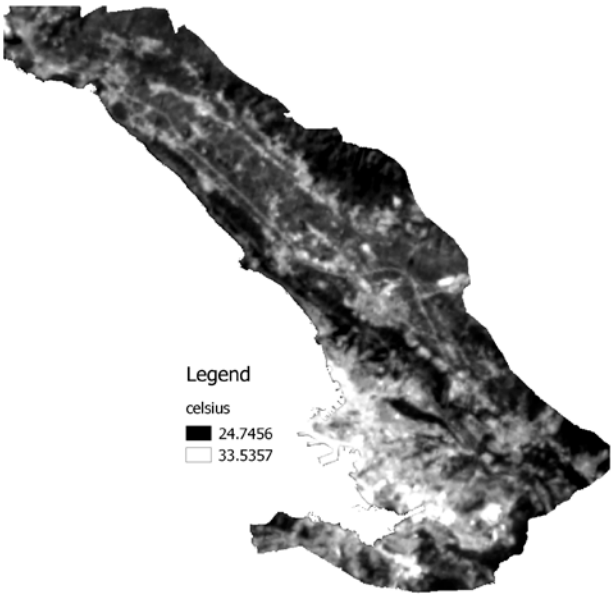

Figure 6. The Land Surface Temperature of the Landsat 8 image (Province of Trieste).

2.5 NDVI layer construction

NDVI, developed by Rouse et al. (1974), is one of the most widely used vegetation index algorithms in remote sensing. NDVI is an efficient index for vegetation monitoring because of its simplicity and close relationship with vegetation productivity (Tucker, 1979).

In order to compute NDVI, the Red and the NIR (Near InfraRed) bands are used. Regarding the OLI images, the equation (3) is:

(3) Band 5 – Band 4/Band 5 + Band 4 (NIR – RED/NIR + RED)

We applied the (3) equation to our OLI image of Trieste Province and we obtained the NDVI layer, which is shown in figure 7.

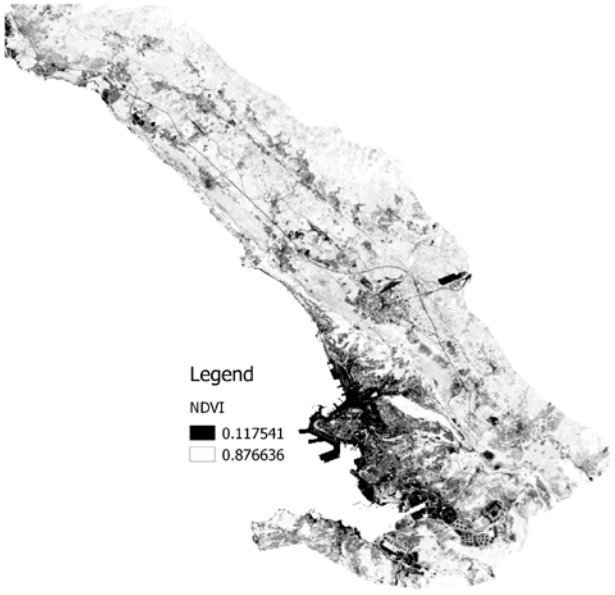

Figure 7. The Normalized Difference Vegetation Index of the Landsat 8 image (Province of Trieste).

3. Results

3.1 Statistical correlation between the layers

In order to investigate the correlation between the above outlined UHI factors, we decided to cluster "Celsius" and "density" as elements which contribute to increasing UHI while we considered "NDVI" and "albedo" as lowering UHI elements.

Then, we summed the layer pixel values, two at a time ("NDVI" plus "albedo" and "Celsius" plus "density").

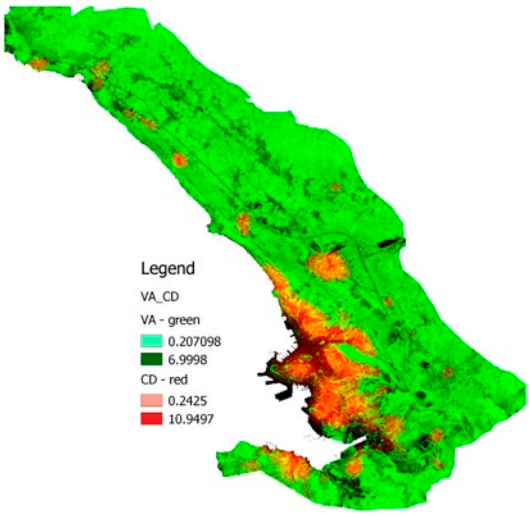

Figure 8. The standardized CD (sum of "Celsius" and "density" layers) and VA (sum of "NDVI" and "albedo" layers) displayed respectively with the red and green channels. (Province of Trieste).

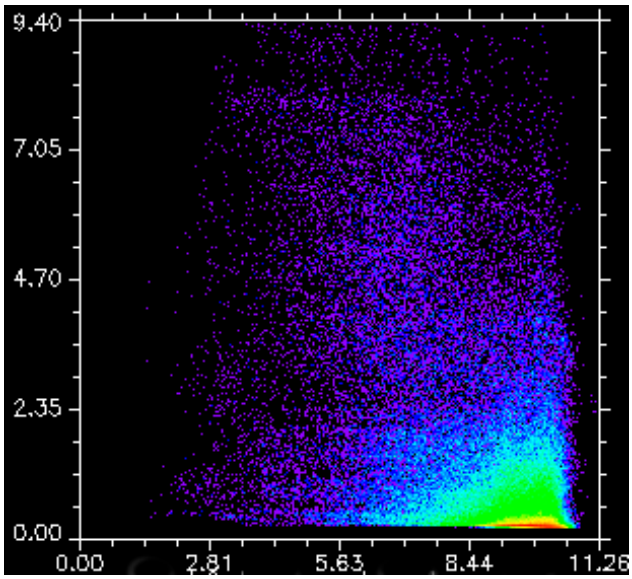

Figure 9. The 2D scatterplot between VA (X axis) and CD (Y axis).

Before the two sums are calculated, we adjust the values of the variables (the pixel values of each layer) in order to bring them in line with each other. In this way we could sum the layer values and keep a true reading. We did this by multiplying the pixels of the "albedo" layer by 0.0001 before summing it with the pixels of the "NDVI" one. Regarding "Celsius" and "density" layers, we summed the pixel values of the two layers and then we multiplied the result by 0.01.

We obtained two layers: one is the sum of "Celsius" and "density" (CD) and the other is the sum of "NDVI" and "albedo" (VA). Figure 8 shows CD and VA layers displayed respectively with the red and green channels. Observing the figure, it is clear that CD values are higher in the urban centers of the province while in the more vegetated karst area there are higher VA values.

The 2D scatter plot between VA (X axis) and CD (Y axis) is shown in figure 9. The different colors in the figure indicate the density of the points in the diagram (from red – high density, to violet – low density).

The inverse correlation between the two variables can be partially identified in the diagram. In order to confirm this visual impression, we made a linear regression analysis between VA and CD.

The resulting regression equation (4) is:

(4) $CD = -4.181 \times VA + 5.078$

the correlation coefficient is: $r = -0.46$
the coefficient of determination is therefore: $r^2 = 0.210$
the Standard Error of the Estimate (SEE) is: SEE = 1.558

Looking at the equation and coefficient values, we can notice the inverse correlation between CD and VA. The resulting correlation coefficient ($r = -0.459$) suggests a moderate degree of correlation (Evans, 1996). The coefficient of determination value is low ($r^2 = 0.210$). As is well known, r^2 describes the fraction of variation in the values of y that is explained by the least-squares regression of y on x (Jain 2010). The obtained SEE is acceptable (it represents the average distance that the observed values fall from the regression line).

In order to broaden the moderate degree of correlation between CD and VA, we checked the correlation degrees between NDVI/Celsius and between albedo/Celsius. Figures 10 and 11 shows respectively these scatterplots (Celsius horizontal axis, NDVI and albedo vertical axis).

As regards the regression equations and coefficients (5 and 6):

- NDVI/Celsius:
  (5) $NDVI = -7.346 \times Celsius + 2.745$
  $r = -0.81$
  $r^2 = 0.662$
  SEE = 0.115
- albedo/Celsius:
  (6) $albedo = 0.330 \times Celsius + 0.070$
  $r = 0.29$
  $r^2 = 0.082$
  SEE = 0.024

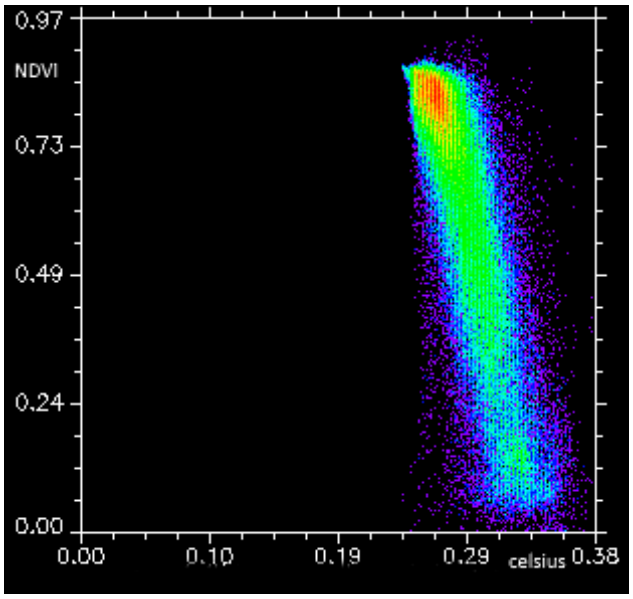

Figure 10. The 2D scatterplot between Celsius (X axis) and NDVI (Y axis).

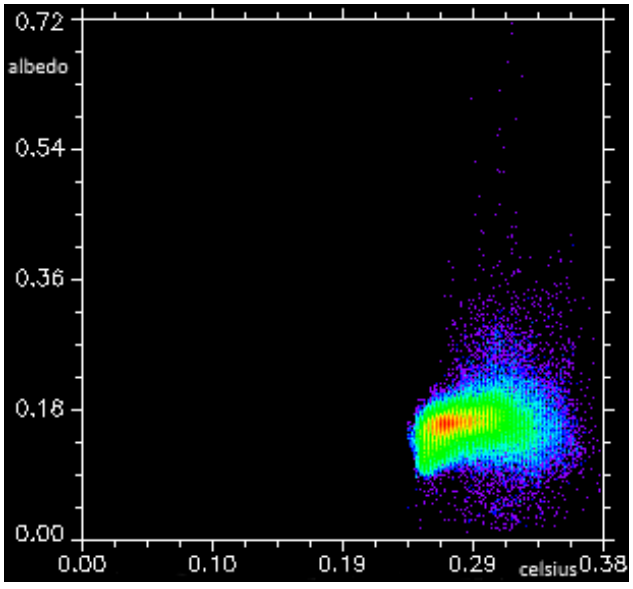

Figure 11. The 2D scatterplot between Celsius (X axis) and Albedo (Y axis).

We can easily observe the very strong inverse correlation between NDVI and temperature. Albedo and temperature unexpectedly have a positive correlation, even if weak. We can try to explain this because of the medium spatial resolution of the OLI sensor (30 meters).

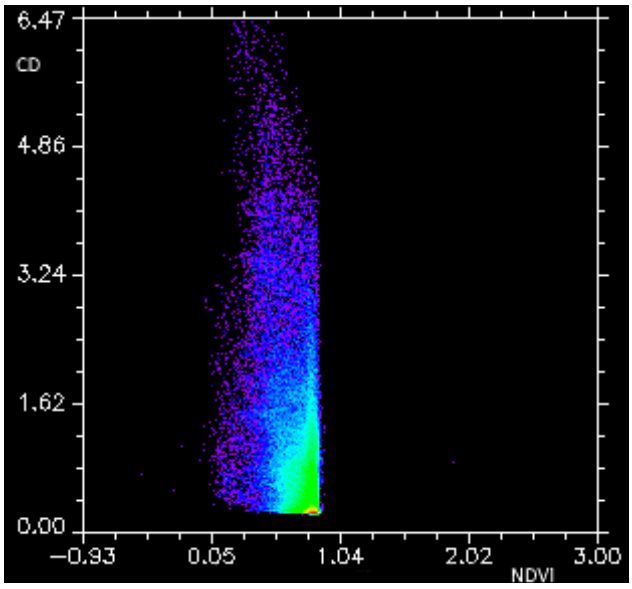

Figure 12. The 2D scatterplot between NDVI (X axis) and CD (Y axis).

In an urban area, the albedo can certainly contribute to lowering the temperature of the buildings, but we think that this cooling effect may be diluted by the extent of the pixel. The overly-large pixel size allows the temperature effect to be higher than the albedo one. Albedo has a cool-down effect on the interior of the buildings and evidently is not registered in the surface temperature by the TIRS sensor.

We decided to remove albedo from the lowering UHI elements and maintain only NDVI. Figure 12 shows the scatter plot between NDVI (X axis) and CD (Y axis) while the new correlation equation (7) and the coefficient parameters are the following:

(7) $CD = -4.157 \times NDVI + 4.384$
$r = - 0.65$
$r^2 = 0.426$
$SEE = 1.55$

Looking at the above coefficients, we can notice a strong inverse correlation between NDVI and CD (even if of lower than that of NDVI /Celsius).

3.2 Some spatial references

In order to locate the variables considered, investigate their relationship and confirm the limited use of the albedo variable in this context, we stacked the four built

layers (density, albedo, Celsius and NDVI) and we classified the stacked layer in an unsupervised manner.

We adopted the ISODATA method to cluster the pixels.[7] The classification results were then refined:

- by a smoothing procedure (kernel size = 3), in order to remove salt and pepper;
- by an aggregation procedure (aggregation minimum size = 9 – in pixel), in order to remove small regions;
- by a raster to vector procedure, in order to export the classified raster layer to a vector file.

Figure 13 shows the stacked layer in a false color visualization (red channel/celsius; green/NDVI; blue/density).

Observing the figure, it is evident that the cemented areas are the hottest ones. Where the density is high, the red becomes purple/light violet. The karst vegetated area is, on the other hand, a lower temperature area, occasionally spaced by a hotter area (quarries, stony karst areas, roads and truck freight terminal).

Figure 14 shows the stacked layer, classified in four classes. The classes are:

- Celsius plus density: it is a class characterized by a high level of temperature and a less high level of density (these are the urban cemented areas and the suburban quarries, stony karst areas, roads and truck freight terminal);
- density plus Celsius: it is a class with a high level of density and high Celsius (urban areas covered by buildings);
- NDVI: it is a class with a predominant vegetation cover and lower levels of density and temperature;
- albedo: this high albedo class was totally cancelled by the clean-up procedure applied, which de facto removed the salt and pepper presence of the high albedo pixel in the classified image.

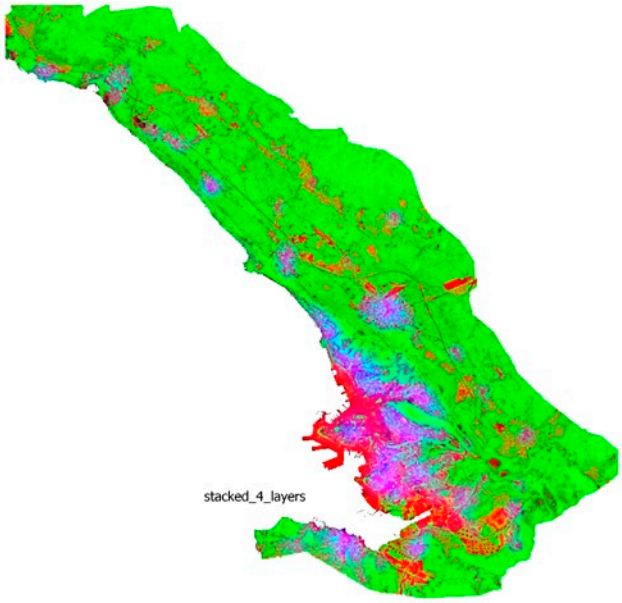

Figure 13. The density, albedo, Celsius and NDVI stacked layer in a false color visualization (red channel/Celsius; green/NDVI; blue/density).

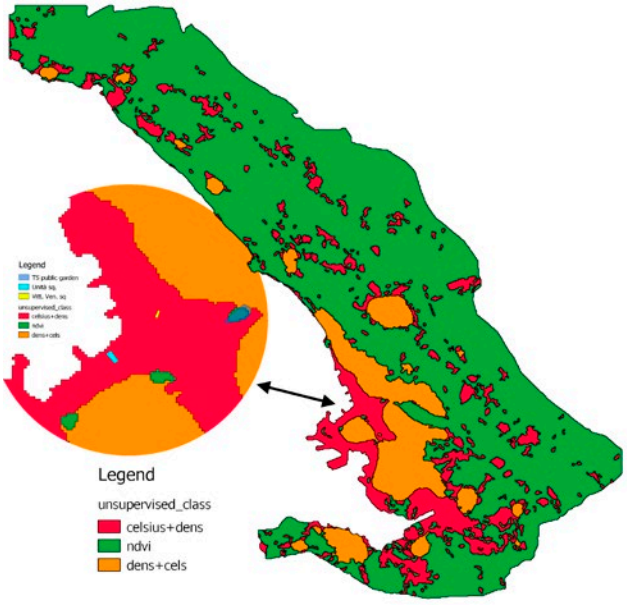

Figure 14. The stacked layer classified in four classes: Celsius plus density; density plus Celsius; NDVI; albedo. The left circle shows a zoomed area of the map in the center of Trieste. Unità and Vittorio Veneto squares (respectively, the light blue and the yellow polygons) are overlaid to the classified map. The blue polygon (visualized with 50% opacity) shows the location the main urban park of the city.

4. Discussion

The work completed on the Landsat 8 satellite image showed two kinds of results. The first were connected to the geography of the studied area while the second were of a methodological kind.

From a geographical point of view, we noticed that in the studied area the higher temperatures were highly correlated to the building density and to the absence of vegetation. This is particularly evident in the urban

[7] As it is well-known, "Cluster analysis is the formal study of methods and algorithms for grouping, or clustering, objects according to measured or perceived intrinsic characteristics or similarity". A brief overview of clustering can be found in Jain (2010).

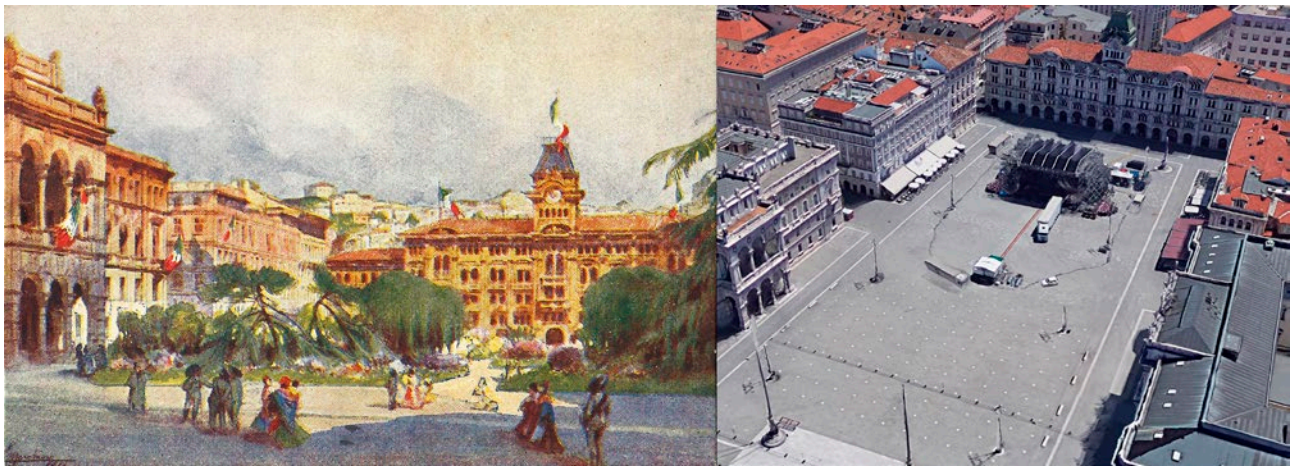

Figure 15. On the left side of the figure: the "Unità" square (city of Trieste), in a historical postcard from about 1910. Source: ICCD, http://www.iccd.beniculturali.it/). On the right side: the current "Unità" square (city of Trieste), from Google Earth (buildings visualization – 2018 Digital Globe).

environment of the city of Trieste (but also occurs in the small villages in the Province). This evidence is closely in line with the results of the main references that have been cited. Looking at Figure 14, we can clearly see that in the urban centers of the province the class "dens+cels" (light brown) is more extended than the class "celsius+dens", which indicates the paved hot urban areas and the stony Karst areas. The green areas in the same figure show the more vegetated urban and Karst areas. Also the lower inverse correlation found between NDVI and CD (celsius+density)[8], compared to the stronger inverse correlation between NDVI and Celsius, suggests that the most efficient UHI reducing policy in the studied area is the increase of urban vegetation.

The gradual replacing of vegetated and permeable soils in the urban environment is unfortunately a constant in modern urban planning policy. Considering the city of Trieste over the last century, we can notice that concrete basements and/or slabs have replaced the gardens and trees in many public squares. See for instance figures 15 and 16.

Figure 15 shows "Unità" square, respectively from a historical postcard (left side - from about 1910) and from Google Earth (right side - buildings visualization – 2018 Digital Globe). It is easy to notice the differences between the two. The historical postcard shows a wooded garden while the 2018 image is a cemented location with no vegetation.

Again figure 16 shows another square in Trieste in the same years as the previous "Unità" square. This is "Vittorio Veneto" square and the location is again covered with vegetation in the historical postcard and cemented in the 2018 image (Google Earth image, buildings visualization – 2018 Digital Globe).

Returning to figure 14, the small circle in the figure shows a close-up of part of the map (in the center of the town). Unità and Vittorio Veneto squares (respectively, the light blue and the yellow polygons) were overlaid onto the classified layer. The blue polygon (visualized with 50% opacity), however, indicates the location of the "Trieste public garden", the main urban park of the city. It is easy to notice that the two squares fell into the "celsius+dens" class while the urban park in the "ndvi" class. We consider this to be in-line with our results, showing that the stacked image is correctly classified and takes account of the true urban land cover.

Another instance of the general widespread lack of knowledge on UHI mitigation factors can be found just by looking at the house facades in Trieste. Figure 17 shows the facade of a house in the city centre.

The facade was once covered by a thriving evergreen ivy that was recently cut in order to repaint the house. The green facades (also called: "living walls") are well known to be UHI mitigation measure because they are "expected to reduce short-wave radiation absorption by the building facade" and in this way "may contribute to the cooling of air temperature around the building via evapotranspiration" (Aleksandrowicz et al. 2017).

[8] The chosen parameters of the building density layer construction may have lowered down the correlation between CD and NA. Further analyses will be made in order to confirm this hypothesis (grid conversion of the building polygons before generating the centroid to be elaborated with the KDE method).

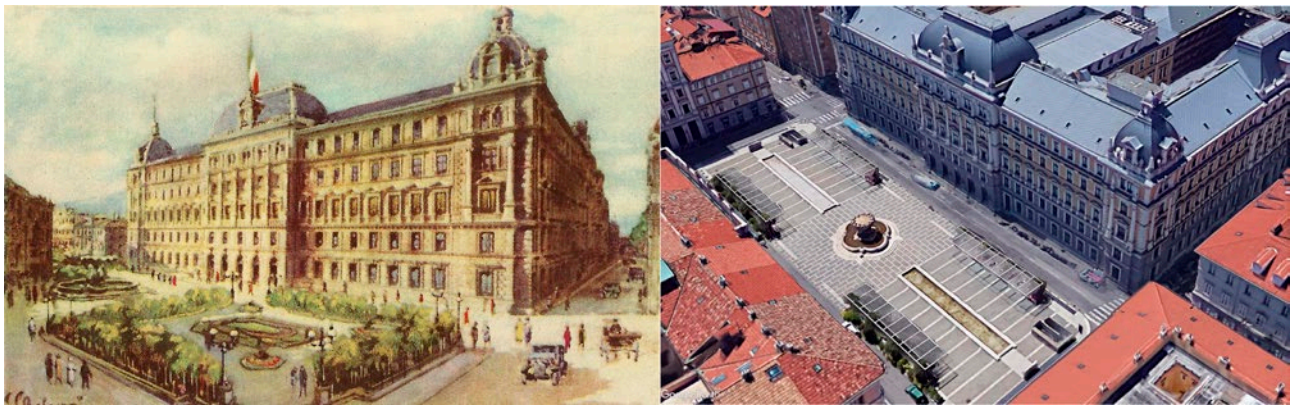

Figure 16. On the left side of the figure: the "Vittorio Veneto" square (city of Trieste), in a historical postcard from about 1910. Source: ICCD, http://www.iccd.beniculturali.it/. On the right side: the current "Vittorio Veneto" square (city of Trieste), from Google Earth (buildings visualization – 2018 Digital Globe).

Figure 17. The facade of a house in Trieste City center. The climbing ivy was recently cut.

From a geographical perspective, we believe that the best and most efficient UHI mitigation policies in the studied province must be the increase of green urban areas. Therefore, we suggest redeveloping all the run down urban areas into public green areas.

From a methodological point of view, we think that our achievements suggest that the spatial resolution of the OLI sensor (30 meters) may obscure the contribution of the albedo as a surface lowering factor in the studied area. At the OLI spatial resolution, albedo values produced a "salt and pepper effect" in the unsupervised classification of the four layer stacked image (the stacked layers were: NDVI, Celsius, albedo and density). This noise effect was almost totally cancelled by the clean-up procedures applied to the raster classified layer (figure 14).

Furthermore, we saw that albedo and Celsius variables were positively correlated. Considering the geography of the studied area, the high reflecting surfaces with higher temperatures must have been the stony Karst areas and the various abandoned quarries close to the main city (Trieste) and the smaller villages of the Province. In the Trieste urban area, these same types of areas were too small to be counted in the classification process, considering the width of the pixel registered by the OLI sensor. Additionally, a high albedo roof can certainly lower the temperature inside the building, but the building surface temperature is still detected as being high by the satellite sensor.

Future research emerging from this study includes the refinement of the KDE procedure to obtain the building density (as previously mentioned) and the verification of the albedo feature with a higher spatial resolution remote sensed image (for instance: a half-meter spatial resolution orto-photo image with a NIR (Near InfraRed) detecting band).

Acknowledgments

Landsat remote sensed imagery courtesy of the U.S. Geological Survey Earth Resources Observation and Science Center.

We thank two anonymous reviewers for their careful reading of our manuscript and their many insightful comments and suggestions.

References

Adinna, E., Christian, E.I., Okolie, A.T. (2009). Assessment of urban heat island and possible adaptations in Enugu urban using Landsat – ETM. *Journal of Geography and Regional Planning*, 2 (2), 30-36.

Aleksandrowicz, O., Vuckovic, M., Kiesel, K., Mahdavi, A. (2017). Current trends in urban heat island mitigation research: Observations based on a comprehensive research repository. *Urban Climate*, 21, 1-26.

Alves, L.E.R., de Freita, I.G.F., Gomes, H.B., dos S. Silva, F.D., dos Santos, M.N. (2017). Using Landsat-8 images in the estimative of surface radiation balance. *Journal of Hyperspectral Remote Sensing*, 7 (2), 91-100.

Amanollahi, J., Abdullah, A.M., Ramli, M.F., Pirasteh, S. (2012). Land Surface Temperature Assessment in Semi-Arid Residential Area of Tehran, Iran Using Landsat Imagery. *World Applied Sciences Journal*, 20 (2), 319-326.

Baldinelli, G., Bonafoni, S., Rotili, A. (2017). Albedo Retrieval From Multispectral Landsat 8 Observation in Urban Environment: Algorithm Validation by in situ Measurements. *IEEE Journal of Selected Topics in Applied Earth Observations and Remote Sensing*, 10 (10).

Bonafoni, S., Baldinelli, G., Verducci, P. (2017). Sustainable strategies for smart cities: Analysis of the town development effect on surface urban heat island through remote sensing methodologies. *Sustainable Cities and Society*, 29, 211-218.

Borruso, G. (2008). Network Density Estimation: a GIS Approach for Analysing Point Patterns in a Network Space. *Transactions in GIS*. 12 (3), 377-402.

Brest, C., Goward, S. (1987). Deriving surface albedo measurements from narrow band satellite data. *International Journal of Remote Sensing*, 3, 351–367.

Chen, F., Yang, S., Yin, K., Chan, P. (2017). Challenges to quantitative applications of Landsat observations for the urban thermal environment. *Journal of Environmental Sciences*, 59, 80-88.

Chen, W., Zhang, Y., Gao, W., Zhou, D. (2016). The Investigation of Urbanization and Urban Heat Island in Beijing Based on Remote Sensing. *Procedia - Social and Behavioral Sciences*, 216, 141-150.

Chen, X.L., Zhao, H.M., Li, P.X., Yin, Z.Y. (2006). Remote sensing image-based analysis of the relationship between urban heat island and land use/cover changes. *Remote Sensing of Environment*, 104, 133-146.

Cristobal, J., Jiménez-Muñoz, J.C., Prakash, A., Mattar, C., Skokovic, D., Sobrino, J. (2018). An Improved Single-Channel Method to Retrieve Land Surface Temperature from the Landsat-8 Thermal Band. *Remote Sensing*, 10, 431, 1-14.

da Silva, B.B., Braga, A.C., Braga, C.C., de Oliveira, L.M.M., Montenegro, S.M.G.L., Barbosa, Junior B. (2016). Procedures for calculation of the albedo with OLI-Landsat 8 images: Application to the Brazilian semi-arid. *Revista Brasileira de Engenharia Agrícola e Ambiental*, 20 (1), 3-8.

Darlington, R.B., Hayes, A.F. (2017). *Regression analysis and linear models*. New York, Guilford Press.

de Faria Peres, L., de Lucena, A.J., Filho, O.C.R., de Almeida França, J.R. (2018). The urban heat island in Rio de Janeiro, Brazil, in the last 30 years using remote sensing data. *International Journal of Applied Earth Observation and Geoinformation*, 64, 104-116.

Deng, Y., Wang, S., Bai, X., Tian, Y., Wu, L., Xiao, J., Chen, F., Qian, Q. (2018). Relationship among land surface temperature and LUCC, NDVI in typical karst area. *Scientific Reports*, 8 (1), 641, 2045-2322.

Duguay, C.R., LeDrew, E.F. (1992). Estimating Surface Reflectance and Albedo from Landsat-5 Thematic Mapper over Rugged Terrain. *Photogrammetric Engineering & Remote Sensing*, 58 (5), 1992, 551-558.

Evans, J.D. (1996). *Straightforward statistics for the behavioral sciences*. Pacific Grove, Brooks/Cole Pub. Co.

Gallo, K.P., McNab, A.L., Karl, T.R., Brown, J.F., Hood, J.J., Tarpley, J.D. (1993). The Use of NOAA AVHRR Data for Assessment of the Urban Heat Island Effect. *Journal of Applied Meteorology*, 32 (5), 899-908.

Gallo, K.P., McNab, A.L., Karl, T.R., Brown, J.F., Hood, J.J., Tarpley, J.D. (1993). The use of a vegetation index for assessment of the urban heat island effect. *International Journal of Remote Sensing*, 14 (11), 2223-2230.

Gondocs, J., Hajnalka, B., Pongracz, R., Bartholy, J. (2017). Urban heat island mesoscale modelling study for the Budapest agglomeration area using the WRF model. *Urban climate*, 21, 66-86.

Grover, A., Singh, R.B. (2015). Analysis of Urban Heat Island (UHI) in Relation to Normalized Difference Vegetation Index (NDVI): A Comparative Study of Delhi and Mumbai. *Environments*, 2, 125-138.

Harlan, S., Ruddell, D. (2011). Climate change and health in cities: impacts of heat and air pollution and potential co-benefits from mitigation and adaptation, Current Opinion. *Environmental Sustainability*, 3, 126–134.

He, T., Liang, S., Wang, D., Cao, Y., Gao, F., Yu, Y., Feng, M. (2018). Evaluating land surface albedo estimation from Landsat MSS, TM, ETM+, and OLI data based on the unified direct estimation approach. *Remote Sensing of Environment*, 204, 181-196.

Jain, A.K. (2010). Data clustering: 50 years beyond K-means. *Pattern Recognition Letters*, 31, 651-666.

Jiménez-Muñoz, J.C., Sobrino, J.A., Skokovic, D., Mattar, C., Cristobal, J. (2014). Land Surface Temperature Retrieval Methods From Landsat-8 Thermal Infrared Sensor Data. *IIEEE Geoscience and Remote Sensing Letters*, 11 (10), 1840-1843.

Keramitsoglou, I., Kiranoudis, C.T., Ceriola, G., Weng, Q., Rajasekar, U. (2011). Identification and analysis of urban surface temperature patterns in Greater Athens, Greece, using MODIS imagery. *Remote Sensing of Environment*, 115, 3080-3090.

Kim, H.H. (1992). Urban heat island. *International Journal of Remote Sensing*, 13 (12), 2319-2336.

Li, Z.L., Wu, H., Wang, N., Qiu, S., Sobrino, J.A., Wan, Z., Tang, B.H., Yan, G. (2013). Land surface emissivity retrieval from satellite data. *International Journal of Remote Sensing*, 34 (9-10), 3084-3127.

Liang, S. (2001). Narrowband to broadband conversions of land surface albedo I algorithms. *Remote Sensing of Environment*, 76, 213-238.

Liang, S. L., Wang, K.C., Zhang, X.T., Wild, M. (2010). Review on estimation of land surface radiation and energy budgets from ground measurement, remote sensing and model simulations. *IEEE Journal of Selected Topics in Applied Earth Observations and Remote Sensing*, 3, 225-240.

Lo, C.P., Quattrochi, D.A., Luvall, J.C. (1997). Application of high resolution thermal infrared remote sensing and GIS to assess the urban heat island effect. *International Journal Remote Sensing*, 18 (2), 287-304.

Mavrogianni, A., Davies, M., Batty, M. (2011). The comfort, energy and health implications of London's urban heat island. *Building Services Engineering Research and Technology*, 32, 35-52.

Menberg, K., Bayer, P., Zosseder, K., Rumohr, S., Blum, P. (2013). Subsurface urban heat islands in German cities. *Science of the total environment*, 442, 123-133.

Mohajerani, A., Bakaric, J., Jeffrey-Bailey, T. (2017). The urban heat island effect, its causes, and mitigation, with reference to the thermal properties of asphalt concrete. *Journal of Environmental Management*, 197, 522-538.

Mohapatra, R.P., Wu, C. (2010). High Resolution Impervious Surface Estimation: An Integration of Ikonos and Landsat-7 ETM Imagery. *Photogrammetric Engineering & Remote Sensing*, 76 (12), 1329-1341.

Moyer, A.N., Hawkins, T.W. (2017). River effects on the heat island of a small urban area. *Urban Climate*, 21, 262-277.

Mushore, T.D., Odindi, J., Dube, T., Matongera, T.N., Mutanga, O. (2017). Remote sensing applications in monitoring urban growth impacts on in-and-out door thermal conditions: a review. *Remote Sensing Applications: Society and Environment*, 8, 83–93.

Nichol, J. (2005). Remote Sensing of Urban Heat Islands by Day and Night. *Photogrammetric Engineering & Remote Sensing*, 71 (5), 613-621.

Nuruzzaman, M. (2015). Urban Heat Island: Causes, Effects and Mitigation Measures. A Review. *International Journal of Environmental Monitoring and Analysis*, 3 (2), 67-73.

O'Malley, C., Piroozfarb, P.A.E., Farr, E.R.P., Gates, J. (2014). An investigation into minimizing urban heat island (UHI) effects: a UK perspective. *Energy Procedia*, 62, 72-80.

Oke, T.R. (1976). City size and the urban heat island. *Atmospheric Environment*, 7, 769-779.

Pimentel, R., Aguilar, C., Herrero, J., Pérez-Palazón, M.J., Polo, M.J. (2016). Comparison between Snow Albedo Obtained from Landsat TM, ETM+ Imagery and the Spot Vegetation Albedo Product in a Mediterranean Mountainous Site. *Hydrology*, 3 (10), 1-19.

Poldini, L., Gioitti, G., Martini, F., Budin, S. (1980). *Introduzione alla flora e alla vegetazione del Carso*. Trieste, Lint.

Rasul, A., Balzter, H., Smith, C., Remedios, J., Adamu, B., Sobrino, J.A., Srivanit, M., Weng, Q. (2017). A Review on Remote Sensing of Urban Heat and Cool Islands. *Land*, 6 (38), 1-10.

Roth, M., Oke, T.R., Emery, W.J. (1989). Satellite-derived urban heat islands from three coastal cities and the utilization of such data in urban climatology. *International Journal of Remote sensing*, 10 (11), 1699-1720.

Rouse, J.W., Haas, R. H., Schell, J.A., Deering, D.W. (1974). Monitoring vegetation systems in the Great Plains with ERTS. In: Fraden, S.C., Marcanti, E.P., Becker, M.A. (eds.). *Third Earth Resources Technology Satellite-1 Symposium*, 10-14 December 1973, Washington DC. NASA.

Santamouris, M. (2011). Using advanced cool materials in the urban built environment to mitigate heat islands and improve thermal comfort conditions. *Solar Energy*, 85, 3085-3102.

Silverman, B.W. (1986). *Density Estimation for Statistics and Data Analysis*. London, Chapman & Hall.

Smith, C, Levermore, G. (2008). Designing urban spaces and buildings to improve sustainability and quality of life in a warmer world. *Energy Policy*, 36, 4558-4562.

Smith, R.B. (2010). *The heat budget of the earth's surface deduced from space*. New Haven (Connecticut), Yale University. Center for Earth Observation https://yceo.yale.edu/sites/default/files/files/Surface_Heat_Budget_From_Space.pdf.

Sun, D., Kafatos, M. (2007). Note on the NDVI-LST relationship and the use of temperature-related drought indices over North America. *Geophisical Research Letters*, 34, L24406, 1-4.

Taha, H. (1997). Urban climates and heat islands: albedo evapotranspiration and anthropogenic heat. *Energy and buildings*, 25 (2), 99-103.

Tucker, C.J. (1979). Red and photographic infrared linear combinations for monitoring vegetation. *Remote Sensing of Environment*, 8 (2), 127-150.

Tzavali, A., Paravantis, J.P., Mihalakakou, G., Fotiadi, A., Stigka, E. (2015). Urban heat island intensity: A literature review. *Fresenius Environmental Bulletin*, 24, 4537-4554.

US Environmental Protection Agency (2008). *Urban Heat Island Basics, in: Reducing Urban Heat Islands: Compendium of Strategies*. Washington D.C, https://www.epa.gov/heat-islands/heat-island-compendium

United Nations (UN) (2016). *The world cities in 2016*. http://www.un.org/en/development/desa/population/publications/pdf/urbanization/the_worlds_cities_in_2016_data_booklet.pdf

US Geological Survey (USGS) (2017). *Earth Resource Observation and Science (EROS) Center Science Processing Architecture (ESPA) on Demand Interface*, Version 3.7.

USGS (2016). *Provisional Landsat 8 Surface Reflectance Code (LaSRC). Product Guide*, Version 3.4.

Vahmani, P., Ban-Weiss, G.A. (2016). Impact of remotely sensed albedo and vegetation fraction on simulation of urban climate in WRF-urban canopy model: A case study of the urban heat island in Los Angeles. *Journal of Geophysical Research: Atmospheres*, 121 (4), 1511-1531.

Vermote, E., Justice, C., Claverie, M., Franc, B. (2016). Preliminary analysis of the performance of the Landsat 8/OLI land surface reflectance product. *Remote Sensing of Environment*, 185, 46-56.

Voogt, J.A., Oke, T.R. (2003). Thermal remote sensing of urban climates. *Remote Sensing of Environment*, 86, 370-384.

Weng, Q. (2001). A remote sensing-GIS evaluation of urban expansion and its impact on surface temperature in the Zhujiang Delta, China. *International Journal of Remote Sensing*. 22 (10), 1999-2014.

Weng, Q. (2009). Thermal infrared remote sensing for urban climate and environmental studies: Methods, applications, and trends. *ISPRS Journal of Photogrammetry and Remote Sensing*, 64, 335-344.

Weng, Q.H., Lu, D.S., Schubring, J. (2004). Estimation of land surface temperature vegetation abundance relationship for urban heat island studies. *Remote Sensing of Environment*, 89, 467-483.

Wittich, K.P. (1997). Some simple relationships between land-surface emissivity, greenness and the plant cover fraction for use in satellite remote sensing. *International Journal of Biometeorology*, 41, 58–64.

Yang, L., Qian, F., Song, D-X., Zheng, K-J. (2016). Research on Urban Heat-island Effect. *Procedia Engineering*, 169, 11-18.

Yang, P., Ren, G., Liu, W. (2013). Spatial and Temporal Characteristics of Beijing Urban Heat Island Intensity. *Journal of Applied Meteorology and Climatology*, 52, 1803-1816.

Yuan, F., Bauer, M.E. (2007). Comparison of impervious surface area and normalized difference vegetation index as indicators of surface urban heat island effects in Landsat imagery. *Remote Sensing of Environment*, 106 (3), 375-386.

Yue, W., Xu, J., Tan, W., Xu, L. (2007). The relationship between land surface temperature and NDVI with remote sensing: application to Shanghai Landsat 7 ETM+ data. *International Journal of Remote sensing*, 28 (15), 3205-3226.

Zeng, Y., Huang, W., Zhan, F.B., Zhang, H., Liu, H. (2010). Study on the urban heat island effects and its relationship with surface biophysical characteristics using MODIS imageries. *Geo-spatial Information Science*, 13 (1), 1-7.

Zhan, W., Chen, Y., Zhou, J., Wang, J., Liu, W., Voogt, J., Zhu, X., Quan, J., Li, J. (2013). Disaggregation of remotely sensed land surface temperature: Literature survey, taxonomy, issues, and caveats. *Remote Sensing of Environment*, 131, 119–139.

Zhan, W., Ju, W., Hai, S., Ferguson, G., Quan, J., Tang, C., Guo, Z., Kong, F. (2014). Satellite-Derived Subsurface Urban Heat Island. *Environmental Science & Technology*, 48 (20), 12134-12140.

Zhang, X.X., Wu, P.F., Chen, B. (2010). Relationship between vegetation greenness and urban heat island effect in Beijing City of China. *Procedia Environmental Sciences*, 2, 1438–1450.